CrossMark
click for updates

Synthesis and adsorption study of hyper-crosslinked styrene-based nanocomposites containing multi-walled carbon nanotubes†

R. Castaldo,[ab] R. Avolio,[a] M. Cocca,[a] G. Gentile,[*a] M. E. Errico,[a] M. Avella,[a] C. Carfagna[a] and V. Ambrogi[ab]

New nanocomposite microporous materials obtained by adding functionalized multi-walled carbon nanotubes (MWCNT) to styrene/vinylbenzyl chloride/divinylbenzene hyper-crosslinked resins were prepared and characterized. In order to promote the embedding of the MWCNT within the gel-type precursor, a suitable surface modification strategy was set up, based on the grafting of a poly(vinylbenzyl chloride) (PVBC) resin, able to participate in the hyper-crosslinking step, onto the nanotube surface. Characterization of the nanocomposites by FTIR spectroscopy and electron microscopy enabled the assessment of the effect of the nanotubes on the structure and the morphology of the resin. Moreover, gas sorption measurements indicated that by addition of nanotubes it is possible to modulate the pore size distribution, the uptake of CO_2 and H_2 and the CO_2/N_2 selectivity. Finally, modified MWCNT are also able to improve the adsorption capacity of phenol from water solutions, suggesting the possible application of the new microporous nanocomposites for water remediation.

Introduction

Porous materials characterized by high specific surface area (SSA) have attracted high scientific interest in recent years. High specific surface area and porosity, in fact, are the fundamental concepts for physical adsorption phenomena. Materials with physical adsorption properties are particularly interesting for their high sorption capacity and their low regeneration energy consumption. Adsorbent materials like activated carbons,[1] zeolites,[2] metal–organic frameworks,[3,4] covalent organic frameworks,[5,6] polymers of intrinsic microporosity,[7] hyper-crosslinked polymers[8] and carbon nanotubes[9] find application in gas separation[10–12] and storage,[13,14] catalysis,[15] and air[16] and water purification processes.[17–19] According to the IUPAC notation, porous materials are defined as microporous when containing pores with characteristic diameter up to 2 nm, mesoporous when having characteristic pores diameter comprised between 2 and 50 nm, or macroporous when being characterized by pores diameter over 50 nm.

Among microporous materials, hyper-crosslinked (HCL) resins stand out for their low density and high chemical and thermal stability[20] and for the possibility of tailoring their structure, porosity, and functionality.[21–23]

The most studied HCL resins are Davankov-type resins, which are prepared by post-crosslinking of polystyrenes.[24–28] One of the synthetic routes to produce them consists in the post crosslinking of linear or lightly crosslinked "gel-type" precursor resins based on styrene (ST), divinylbenzene (DVB) and vinyl-benzyl chloride (VBC). The precursor resin is usually prepared by suspension polymerization, then through post crosslinking various structural bridges between neighbouring phenyl groups are obtained. The hyper-crosslinking process leads to a highly porous three-dimensional network, which displays high specific surface area and excellent sorption properties.

In particular, this class of micro/mesoporous materials is characterized by high crosslinking degree, small average pore diameter (lower than 3 nm), high BET surface area (up to about 1800 m^2 g^{-1}), and large pore volume (up to 0.8 cm^3 g^{-1}).[28]

A recent review of Fontanals *et al.*[26] well summarizes the structural and adsorption properties of HCL polystyrene resins. In particular, several studies have been focused on the effect of the compositions of DVB, ST and VBC on the final properties of the hyper-crosslinked product.[29] In fact, the degree of cross-linking in the gel-type precursor can be modulated by varying the DVB content, whereas changing the molar ratio between ST and VBC, and thus the relative amount of chloromethyl groups in the gel-type precursor, significantly affects the extent of the hyper-crosslinking. Within this class of materials, the highest specific surface is reported for the system obtained by using 2 mol% of DVB and 98 mol% of VBC.[30]

Moreover, in the last years, several modification strategies have been proposed to improve the overall adsorption properties

a Institute for Polymers, Composites and Biomaterials, National Research Council of Italy, Via Campi Flegrei 34, 80078 Pozzuoli, Italy. E-mail: gennaro.gentile@cnr.it

b Department of Chemical, Materials and Production Engineering, University of Naples, Piazzale Tecchio 80, 80125 Napoli, Italy

of HCL resins, to find alternative monomer compositions, including the use of bioderived monomers/macromers, or to add specific functionalities to the final materials with the objective of imparting selectivity towards the absorption of selected gases or low molecular weight substances. Jia et al.[31] have recently evaluated the effect of the solvent used during the hyper-crosslinking step on the surface properties and the adsorption properties of ST/VBC/DVB resins, showing that, also based on environmental and economic considerations, 1,2-dichloroethane is a better option with respect to nitrobenzene. Li et al.[32] have synthesized a carbonyl modified VBC-based resin, characterized by improved adsorption properties toward an aromatic substance containing hydroxyl groups, i.e. glabridin, an isoflavonoid, from water solutions. Following the studies of Zeng et al.[33–35] that synthesized a series of polar-modified post-crosslinked polystyrene, Ling et al.[36] have recently developed a highly polar HCL resins based on DVB and glycidylmethacrylate, characterized by improved adsorption of salicylic acid from water.

As concerning the use of bioderived raw materials, Meng and Weber[37] have recently realized a novel microporous polymer by hyper-crosslinking of organosolv lignin, that, after pyrolysis, shows good carbon dioxide adsorption and excellent CO_2/N_2 selectivity.

Other methods for the modification of sorption properties of HCL resins are based on the embedding of micro/nanoparticles within the polymer network. Wang W. et al.[38] synthesized a magnetic DVB-based HCL resin filled with needle-like γ-Fe_2O_3 particles, showing that the realized composite resin is suitable for rapid and efficient removal of organic pollutants from drinking water.

In this context, carbon nanomaterials, due to their intrinsic adsorption properties,[39–42] are very interesting candidates to modulate the properties of HCL resins. In particular, carbon nanotubes (CNT) are effective in CO_2 adsorption[43] and in removing organic and inorganic pollutants from air[44,45] or from water.[46,47] The high adsorption capacity of CNT is mainly attributed to their porous structure. Furthermore, CNT surface can be modified by chemical modification or thermal treatments, introducing functional groups that can enhance the selective adsorption toward specific substances.[48]

On this basis, in this work properly modified multi-walled carbon nanotubes (MWCNT) were for the first time incorporated into a ST/VBC/DVB HCL resin. The interaction of the fillers with the hosting matrix, and their effect on the structure of the resin, the morphology, the specific surface area and porosity have been investigated. Furthermore, adsorption of phenol from water solution has been evaluated as a function of the composition of the resin and the amount of nanotubes.

Experimental section

Materials

CVD-grown MWCNT functionalized with –COOH groups (MWCNT-COOH, purity >95%, functionality 0.7 wt%, diameter range 20–50 nm) were purchased from Cheap Tubes Inc. (Brattleboro, VT, USA).

Polyvinyl alcohol (PVA, Mowiol® 18–88, $M_w \sim 130\,000$, 86.7–88.7 mol% hydrolysis), NaCl (>99%, anhydrous), NaOH (≧97.0%, pellets), tetraoctylammonium bromide (TOAB, >98%), styrene (ST, >99.9%), 2,2′-azobis(2-methylpropionitrile) (AIBN, >98%), vinylbenzyl chloride (VBC, ≧95.0%, mixture of isomers, ~70% meta + ~30% para), p-divinylbenzene (DVB, 85%, meta isomer, ~10 wt%), $FeCl_3$ (≧97%), phenol (>99.5%) and all solvents were purchased from Sigma Aldrich (Milan, Italy) and used without further purification.

Multi-walled carbon nanotubes surface modification

Carboxyl groups modified multi-walled carbon nanotubes (MWCNT-COOH) were functionalized by grafting their external surfaces with poly(vinylbenzyl chloride) (PVBC).[49]

PVBC was obtained by solution polymerization using the following procedure. VBC (5 mL) was poured in a round-bottom flask filled with toluene (10 mL). AIBN (0.054 g) was added, the solution was heated to 60 °C and the reaction was carried out under reflux and under nitrogen for 14 hours. PVBC was precipitated in ethanol and dried under vacuum overnight.

MWCNT-COOH (600 mg) were poured into 350 mL of a NaOH aqueous solution (0.005 M) and stirred for 15 minutes. Then 1 g of TOAB was added and the mixture was heated to 60 °C. PVBC (300 mg), pre-dissolved in 250 mL of toluene, was added to the mixture. The reaction was carried for 7 hours under vigorous stirring, after that the mixture was poured in a separatory funnel and the toluene phase was recovered and filtered. Modified MWCNT (MWCNT-PVBC) were purified from unreacted reagents by 3 washing cycles with chloroform and tetrahydrofuran, then they were dried in oven at 50 °C for 24 hours.

Synthesis of the precursor gel-type resin by suspension polymerization

Poly(divinylbenzene-co-styrene-co-vinylbenzyl chloride) beads were obtained by suspension polymerization, using the following procedure.[25] A PVA (7.5 g L^{-1}) and NaCl (33 g L^{-1}) water solution (350 mL) was poured into a suspension polymerization reactor fitted with a water condenser and a mechanical stirrer. The organic phase, composed of DVB, ST, VBC in two different molar compositions, 2 : 0 : 98 and 2 : 49 : 49, and 0.5 phr of AIBN, was mixed and maintained for 30 min under nitrogen; then it was poured drop by drop in the aqueous phase (in a ratio of 20 : 1 wt/wt of aqueous phase : organic phase) under stirring at 425 rpm. The reaction was carried out under nitrogen at 80 °C for 6 h. The obtained beads were recovered on a 75 μm sieve and washed with 5 washing cycles of water and methanol. Then, the beads were further purified by Soxhlet extraction with acetone to eliminate remaining impurities. Finally, they were washed with methanol and diethyl ether on a paper filter and dried in a vacuum oven at 40 °C for at least 24 h.

Beads containing MWCNT-PVBC were prepared using a similar procedure. In this case, before reaction, the right amount of modified nanotubes (1.5 and 3.0 phr) was dispersed within the organic phase by sonication for 50 minutes, with

a 500 W tip sonicator at the 25% power, with a 10 s/50 s ON/OFF cycle, under nitrogen. The initiator (AIBN), 0.5 phr, was then added and the whole mixture was poured drop by drop into the aqueous solution of PVA and NaCl. The obtained nanocomposite beads were washed and dried following the procedure used for the neat polymer beads.

Hyper-crosslinking of the gel-type resin

The hyper-crosslinking reaction was performed using the following procedure.[30] The precursor resin was swollen in 1,2-dichloroethane (DCE), under nitrogen, for 2 h. Then the mixture was cooled to ~4 °C in an ice bath, and the Friedel–Crafts catalyst, $FeCl_3$, was added. After allowing 2 h to achieve a uniform dispersion of $FeCl_3$ throughout the precursor beads, the temperature was raised to 80 °C and kept for 18 h. The hyper-crosslinked beads were then washed with methanol and dried in a vacuum oven for a day at 40 °C.

MWCNT-PVBC characterization

The extent of the functionalization of the multi-walled carbon nanotubes by grafting of PVBC was evaluated by means of Fourier transform infrared spectroscopy (FTIR) analysis, energy dispersive X-ray analysis (EDX), thermogravimetric analysis (TGA) and transmission electron microscopy (TEM).

FTIR spectra were recorded on the neat PVBC resin, on pristine MWCNT-COOH, and on MWCNT-PVBC with a Perkin Elmer Spectrum One FTIR spectrometer. Spectra were collected using a resolution of 4 cm^{-1} and 32 scan collections.

EDX analysis was performed on a FEI Quanta 200 FEG SEM equipped with an Oxford Inca Energy System 250 and an Inca-X-act LN2-free analytical silicon drift detector. A thin layer of pristine MWCNT-COOH and MWCNT-PVCB was deposited onto aluminium SEM stubs. The analysis was performed at 30 kV acceleration voltage. Average results and standard deviation values are based on three consecutive measurements on different areas of each sample.

TGA was performed on pristine and modified MWCNT with a Perkin Elmer Pyris Diamond TG/DTA analyzer, using nitrogen as purge gas (50 mL min^{-1}), heating about 3 mg of each sample from 100 to 900 °C at 2 °C min^{-1}.

Bright field TEM analysis of MWCNT-COOH and MWCNT-PVBC was performed on a FEI Tecnai G12 Spirit Twin (LaB$_6$ source) at 120 kV acceleration voltage. TEM images were collected on a FEI Eagle 4k CCD camera. Before the analysis, pristine MWCNT-COOH were dispersed in water and MWCNT-PVBC in toluene by sonication (2 min) with a 500 W tip sonicator set at 25% power. Carbon nanotubes were then collected by immersing holey carbon coated copper grids in the dispersion.

Furthermore, in order to prove the ability of the grafted PVBC phase to undergo the Friedel–Crafts reaction, MWCNT-PVBC were subjected to hyper-crosslinking following the procedure already described for gel-type resins and obtaining the sample coded X_MWCNT-PVBC. This sample was characterized by FTIR spectroscopy, EDX and TGA, as above detailed.

Moreover, SSA was determined on pristine MWCNT-COOH, MWCNT-PVBC and MWCNT-PVBC through N_2 adsorption analysis performed at liquid nitrogen temperature using a Micromeritics ASAP 2020 analyzer. Prior to the analysis all the samples were degassed at 120 °C under vacuum ($P < 10^{-5}$ mbar). SSA was determined from the linear part of the Brunauer–Emmett–Teller (BET) equation.

Precursor beads characterization

Precursor beads were characterized by FTIR and morphological analysis. ATR-FTIR spectra were recorded on the neat precursor and nanocomposite beads with the above described FTIR apparatus, equipped with a universal ATR sampling accessory, using a resolution of 4 cm^{-1} and 32 scan collections.

Scanning electron microscopy (SEM) of the beads was performed by means of a FEI Quanta 200 FEG SEM in high vacuum mode. Before SEM observations, samples were mounted onto SEM stubs by means of carbon adhesive disks and sputter coated with a 15 nm thick Au–Pd layer. External surfaces as well as beads cross-sections were observed for all the samples at 10–30 kV acceleration voltage using a secondary electron detector.

HCL resins and nanocomposites characterization

To confirm the extent of the hyper-crosslinking reaction, ATR-FTIR and EDX analysis was performed on the HCL samples using the above described equipment and experimental conditions.

Gas adsorption volumetric measures were performed on the HCL samples using a Micromeritics ASAP 2020 analyzer. All the adsorption measurements were performed using high purity gases (>99.999%). Prior to the analysis all the samples were degassed at 120 °C under vacuum ($P < 10^{-5}$ mbar) in the degas port of the analyzer. In particular, N_2 adsorption analysis was performed at liquid nitrogen temperature to evaluate the SSA and the pore size distribution of the samples. SSA was determined from the linear part of the Brunauer–Emmett–Teller (BET) equation. Non-local density functional theory (NLDFT) was applied to nitrogen adsorption isotherm curves to evaluate the pore size distribution of the materials.[50] N_2 and CO_2 adsorption analysis were performed at 298 K up to 1 bar, and the equilibrium selectivity of the materials towards CO_2 with respect to N_2 was evaluated as the ratio of the absolute adsorption values. H_2 uptake capacity was evaluated at 77 K up to 1 bar.

Equilibrium phenol adsorption in water was performed at 25 °C in the range of phenol concentrations 200–1500 mg L^{-1}. About 10 mg of HCL resins or nanocomposites were introduced into vials containing 10 mL of phenol solution at different concentrations. The vials were kept at 25 °C until equilibrium was reached (at least 48 h). Therefore, the solution was removed from the vial and the final phenol concentration was measured using a Jasco V570 UV spectrophotometer. A calibration curve was built to determine the phenol concentration in water from the absorbance of the peak centred at 270 nm.

a mixture of plain MWCNT and 8.8 wt% of PVBC would result in a chlorine/carbon weight ratio of 2.12%. Therefore, it can be deduced that only about 16% of the chlorine atoms of PVBC are replaced during the grafting reaction and then a large amount of residual chloromethyl groups of MWCNT-PVBC are still available for further reactions.

As detailed in the experimental, in order to confirm that the PVBC phase grafted onto modified carbon nanotubes is able to participate to the HCL reaction when nanotubes are embedded into the precursor resin, hyper-crosslinking of the modified nanotubes was performed using the procedure reported for the resin and nanocomposite beads. FTIR analysis of the obtained X_MWCNT-PVBC sample confirmed the occurrence of the hyper-crosslinking reaction. In fact, as shown in Fig. 2b, a significant decrease of the intensity of the absorption band centered at 1265 cm^{-1} was recorded for X_MWCNT-PVBC in comparison to the MWCNT-PVBC sample, proving that the chloromethyl groups of the grafted PVBC can undergo the Friedel–Crafts reaction. EDX analysis further confirmed this result, as the residual chlorine/carbon weight ratio decreased from 1.78 ± 0.38 of MWCNT-PVBC to 0.68 ± 0.22 of X_MWCNT-PVBC. Although FTIR and EDX indicated that the extent of the hyper-crosslinking was not complete, it was expected that a highly microporous layer could be obtained on the surface of the modified nanotubes, due to the presence of a partially HCL phase, thus inducing a significant increase of the SSA of the X_MWCNT-PVBC with respect to the unmodified MWCNT-COOH and to the non-hyper-crosslinked MWCNT-PVBC. BET analysis confirmed the increase of SSA from 113.7 ± 0.7 m^2 g^{-1} and 108.5 ± 0.6 m^2 g^{-1} for MWCNT-COOH and MWCNT-PVBC, respectively, to 140.8 ± 0.3 m^2 g^{-1} for X_MWCNT-PVBC. As the increase of SSA can be only due to the hyper-crosslinking of the grafted PVBC, based on geometric considerations it is possible to estimate the SSA of the grafted and hyper-crosslinked polymer phase. Therefore, hypothesizing a perfect cylindrical geometry of the nanotubes, a nanotube radius of 25 nm, a constant thickness of the grafted PVBC layer of 2.0 nm, and assuming density values of 2.1 g cm^{-3} for the nanotubes and 1.34 g cm^{-3} for the HCL PVBC phase,[8] the recorded increase corresponds to the formation of a HCL PVBC layer with SSA of about 400 m^2 g^{-1}. This value is very low in comparison to SSA obtained for VBC based HCL Davankov type resins (up to 1800 m^2 g^{-1}), but, in agreement with FTIR and EDX results, can be easily explained considering the low mobility of the grafted PVBC phase that, in the case under consideration, is constrained on the nanotube surface, thus precluding the possibility of achieving a high extent of hyper-crosslinking.

Synthesis of the gel-type precursors by suspension polymerization

The synthesis of gel-type precursor beads was performed by radical suspension polymerization starting from two different mixtures of monomers, DVB : VBC = 2 : 98 molar ratio and DVB : ST : VBC = 2 : 49 : 49 molar ratio, coded as DVB–VBC and DVB–ST–VBC, respectively. Nanocomposite beads were realized using the same monomer compositions and adding 1.5 and 3.0

phr of MWCNT-PVBC, thus obtaining the samples coded as DVB–VBC_1.5CNT, DVB–VBC_3CNT, DVB–ST–VBC_1.5CNT and DVB–ST–VBC_3CNT. In all cases, lightly crosslinked beads were produced, where the low amount of crosslinks is due to the bifunctional DVB monomer.

In Fig. 3 ATR-FTIR spectra of gel type precursors and hyper-crosslinked resins and nanocomposites are reported. These latter will be discussed in the next section. As concerning the gel type precursors, DVB–VBC and DVB–ST–VBC spectra show the absence of residual double bonds and the presence at 1265 cm^{-1} of the absorption band diagnostic for the chloromethyl groups of the VBC unit. Of course, the ATR-FTIR spectrum of DVB–ST–VBC is characterized by a lower intensity of the chloromethyl absorption band due to the lower relative amount of VBC.

FTIR spectra of the corresponding gel-type nanocomposites containing 1.5 and 3.0 phr of MWCNT-PVBC, not reported in Fig. 3, did not show significant differences with respect to the unfilled resins, thus indicating that MWCNT-PVBC do not negatively affect the synthesis of the gel type precursors.

SEM images of the gel-type resins and nanocomposite beads are reported in Fig. 4 and 5. As it can be observed, all the beads have a spherical shape, their diameter ranging between 100 and 400 μm, irrespectively of the presence of nanotubes. As

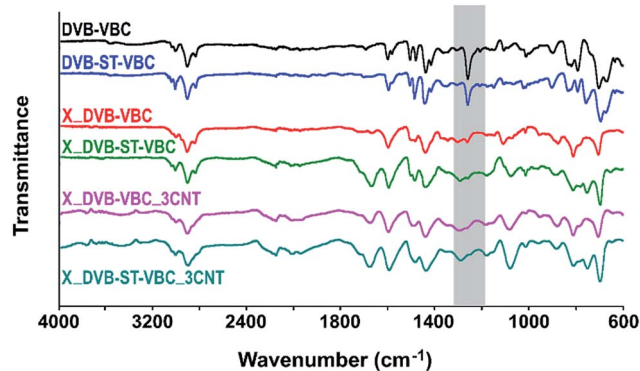**Fig. 3** ATR-FTIR spectra of the gel type precursor resins (DVB–VBC and DVB–ST–VBC), the corresponding hyper-crosslinked resins (X_DVB–VBC and X_DVB–ST–VBC) and nanocomposites containing 3 phr of MWCNT-PVBC (X_DVB–VBC_3CNT and X_DVB–ST–VBC_3CNT).
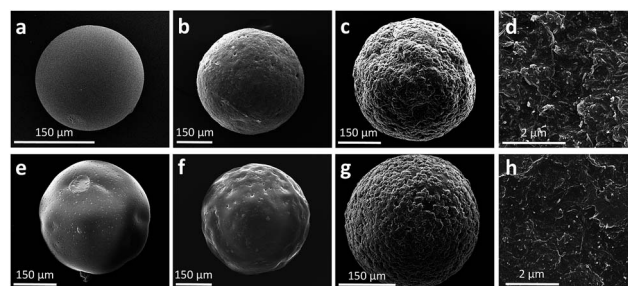

Fig. 4 SEM micrographs of the precursor beads: DVB–VBC (a), DVB–VBC_1.5CNT (b), DVB–VBC_3CNT (c and d), DVB–ST–VBC (e), DVB–ST–VBC_1.5CNT (f), DVB–ST–VBC_3CNT (g and h).
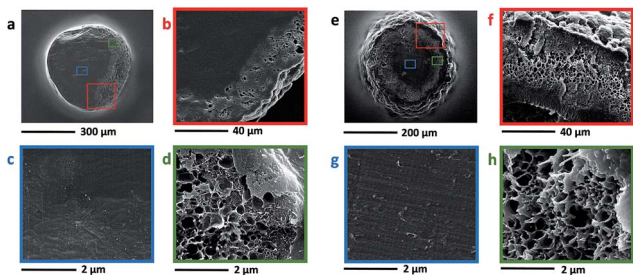
Fig. 5 SEM micrographs of sections of the precursor beads: DVB–VBC_3CNT (a–d), DVB–ST–VBC_3CNT (e–h).

concerning the external morphology, neat DVB–VBC and DVB–ST–VBC beads (Fig. 4a and e) show a smooth surface, while an increased roughness was recorded for both compositions increasing the relative amount of MWCNT-PVBC. This roughness is attributed to the presence of appreciable amounts of nanotubes on the beads surface, as shown by high magnification SEM images in Fig. 4d (DVB–VBC_3CNT) and 4 h (DVB–ST–VBC_3CNT).

In order to evaluate the distribution within the whole volume of the beads, SEM analysis was also performed on the beads sections (see Fig. 5). In stark contrast with the smooth and plain section of the neat beads observed for both compositions (see Fig. S2†), all the samples containing MWCNT-PVBC show a complex structure, almost irrespectively of the nanotube content.

In particular, as shown in Fig. 5 for the samples containing 3 phr of MWCNT-PVBC, just under the external corrugated layer of the beads, a macroporous layer with cylindrical pores of 300–400 nm diameter is evidenced, containing MWCNT-PVBC (Fig. 5d and h). Finally, a dense core containing a lower amount of MWCNT-PVBC with respect to the external layer, is shown in Fig. 5c and g.

The obtained results confirm the uneven distribution of MWCNT, that is an interesting phenomenon already observed in different systems, such as immiscible polymer blends[53] and water/paraffin emulsions. In the latter case, wax microparticles in which carbon nanotubes are selectively located at the particles surfaces have been obtained by cooling of water/paraffin wax Pickering emulsions.[54] The partially selective localization of the MWCNT at the surface of the gel-type precursor beads is expected to affect the adsorption properties of the HCL nanocomposites.

HCL resins and nanocomposites characterization

For the investigated class of materials, the hyper-crosslinking of the precursor beads was performed in a solvent-swollen state by using DCE,[31] through the reaction of the chloromethyl groups of the VBC monomer, inducing the formation of methylene bridges between neighbouring aromatic rings of the resin. Hyper-crosslinking preserves the porosity even when the swelling solvent is removed and thus provides high specific surface area to the materials.[55] As already stated, for the systems containing MWCNT-PVBC, modified nanotubes are able to participate to the hyper-crosslinking reaction with the precursor

resin through the chloromethyl groups of the grafted PVBC resin. This can induce the formation of a highly interconnected network of resin and nanotubes, which, in combination with the particular morphology and structure of the precursor beads containing modified nanotubes, supported the hypothesis that the addition of MWCNT-PVBC can affect the porosity and the adsorption properties of the HCL resin.

ATR-FTIR and EDX analysis. The extent of the hyper-crosslinking reaction in the investigated systems was verified by means of ATR-FTIR analysis. As shown in Fig. 3 for the resins X_DVB–VBC and X_DVB–ST–VBC, the almost complete disappearance of the sharp absorption band centered at 1265 cm^{-1} (evidenced with the grey rectangle in Fig. 3), characteristic of the CH$_2$Cl group, confirmed the occurrence of the hyper-crosslinking. A similar behavior was also observed for all the samples containing MWCNT-PVBC, as shown in Fig. 3 for nanocomposites X_DVB–VBC_3CNT and X_DVB–ST–VBC_3CNT. EDX analysis performed on the HCL samples confirmed the occurred reaction, revealing for all the investigated systems a residual chlorine content close to 1.5–2.0 wt%, with no significant differences amongst the samples. In agreement with FTIR results, this value, compared to the original chlorine contents of about 13 and 22 wt% of the DVB–ST–VBC and DVB–VBC based resin and nanocomposite precursors, respectively, indicates the large extent of the hyper-crosslinking.

Moreover, in Fig. 3 are also evident, for the HCL resins and for the nanocomposites containing 3 phr of surface modified CNT, complex absorption bands in the wavenumber range 1650–1780 cm^{-1}. These bands are much more intense in the case of systems obtained by the DVB–ST–VBC precursors.

In previous studies,[56] for HCL reactions carried out in nitrobenzene, these absorption bands have been attributed to the oxidation of chloromethyl groups to carbonyl ones promoted by the solvent and further oxidation of the carbonyls to carboxyl groups promoted by oxygen. In our case, we used DCE as a swelling medium for the HCL reaction, and therefore the presence of large amounts of carboxyl groups was unexpected. A detailed explanation of the presence of absorption bands in the range 1600–1740 cm^{-1} for HCL Davankov-type resins was reported by Tsyrupa et al.,[57] that denied the presence of C=O functionalities in the HCL polystyrenes, attributing these bands to hindered vibrations of carbon–carbon bonds and valence angles in aromatic rings. In our case, the hypothesis denying the dependence of these bands on C=O groups is confirmed by EDX results on the HCL systems that have evidenced comparable oxygen contents, 3.72 ± 0.13 mol% and 3.55 ± 0.23 mol%, for X_DVB–VBC and for X_DVB–ST–VBC, respectively, with no significant differences recorded for the corresponding nanocomposites. Although this subject is outside the scope of this work, further investigations would be needed to explain why the intensity of these absorption bands is higher for the systems with the lower VBC content with respect to the DVB–VBC systems.

Specific surface area and pore size distribution. Results of the BET SSA and DFT analysis of the HCL resins and nanocomposites are reported in Table 1. As it can be observed by the nitrogen absorption/desorption isotherms at 77 K in Fig. 6, all

Table 1 Results of SSA and pore size distribution analysis, CO_2 uptake, CO_2/N_2 selectivity and H_2 uptake

Sample	BET SSA ($m^2\ g^{-1}$)	Microporosity fraction (%)	Micropores volume ($cm^3\ g^{-1}$)	Total pore volume ($cm^3\ g^{-1}$)	CO_2 uptake[a] (wt%)	CO_2/N_2 selectivity[b]	H_2 uptake[c] (wt%)
X_DVB–VBC	1715 ± 4	32	0.39	1.21	2.99	10.5	1.11
X_DVB–VBC_1.5CNT	1743 ± 18	64	0.54	0.84	3.55	11.0	1.39
X_DVB–VBC_3CNT	1750 ± 4	28	0.38	1.36	3.46	13.6	1.35
X_DVB–ST–VBC	1219 ± 6	37	0.31	0.83	3.26	14.8	1.08
X_DVB–ST–VBC_1.5CNT	1189 ± 9	47	0.34	0.72	3.46	20.9	1.04
X_DVB–ST–VBC_3CNT	1069 ± 7	38	0.28	0.74	2.61	19.8	1.09

[a] Measured at 298 K and 750 mmHg. [b] Calculated at 298 K and 100 mmHg. [c] Measured at 77 K and 750 mmHg.

the materials present a type II isotherm, with hysteresis in desorption attributed to the solubility of nitrogen in the HCL polymer.[58]

The obtained HCL materials show two different ranges of specific surface area. The set of HCL resins and nanocomposites obtained by the DVB–VBC systems have SSA values of 1700–1750 $m^2\ g^{-1}$, whereas the samples prepared from the DVB–ST–VBC show SSA values of 1000–1200 $m^2\ g^{-1}$. This difference was already reported,[8,29,30] and it is explained considering the high amount of chloromethyl groups in the DVB–VBC class of materials, and thus their higher potentiality to induce the formation of methylene bridges between adjacent aromatic rings with respect to the DVB–ST–VBC systems.

By addition of MWCNT-PVBC, only a slight increase of the SSA was obtained for the DVB–VBC system, while for the DVB–ST–VBC resins the SSA was not significantly influenced by addition of 1.5 phr of MWCNT-PVBC and decreased from 1219 to 1069 $m^2\ g^{-1}$ at 3.0 phr nanotube loading.

Instead, the presence of modified nanotubes significantly influence the porosity of the resins. Applying the NLDFT to the nitrogen absorption isotherm curves and assuming a slit pore geometry, all systems are characterized by micro- and mesoporosity, with pore diameters basically up to 10 nm. For both the investigated monomer compositions, HCL nanocomposites containing 1.5 phr of MWCNT-PVBC showed a reduction of the total pore volume and an appreciable increase of the microporosity fraction, as reported in Table 1. In particular, X_DVB–VBC_1.5CNT resulted in the highest microporosity fraction (0.64), which is also noticeable from the shape of the nitrogen absorption isotherm. In fact, for this sample the nitrogen adsorption mainly occurs at relative pressure $p/p_0 <$ 0.3, and in this region the gas adsorption is ascribed to the smallest pores. With increasing the pressure, the sample was not able to adsorb a further significant volume of nitrogen, confirming the presence of a reduced number of mesopores. X_DVB–VBC_1.5CNT also exhibited the smallest hysteresis loop, and this phenomenon is in agreement with the thermodynamic theory stating that the hysteresis area decreases with the decreasing of the pore size.[59,60]

By increasing the nanofiller loading to 3.0 phr a reduction of the microporosity with respect to the systems containing 1.5 phr of MWCNT-PVBC was recorded. This effect can be ascribed to the preferential localization of the nanotubes on the beads surface during the polymerization of the precursor, as shown by morphological analysis. This phenomenon induces the formation of nanotube clusters, whose dimension increases with increasing the overall nanotube amount. Agglomeration of nanotubes can inhibit the extensive hyper-crosslinking between the PVBC resin grafted on the nanotube and the bulk resin, thus leading to an increase of the mesoporosity fraction.

CO_2 uptake and CO_2/N_2 selectivity. Physisorption is considered a promising technology for CO_2 capture, offering possible energy savings compared to other more established absorption technologies. In this view, microporous hyper-crosslinked resins are interesting candidates for CO_2 capture, and currently different research efforts aim at improving the selectivity of CO_2 sorption with respect to N_2.[61]

Results obtained on the investigated systems from CO_2 and N_2 adsorption tests at 298 K and CO_2/N_2 absorption selectivity at low pressure are reported in Table 1. CO_2 absorption values recorded for the HCL resins and nanocomposites are in agreement with the literature values for microporous polymers, confirming that there is not a direct correlation between SSA and CO_2 adsorption. In fact, as evidenced in Table 1, despite to the large differences observed in the SSA, comparable CO_2
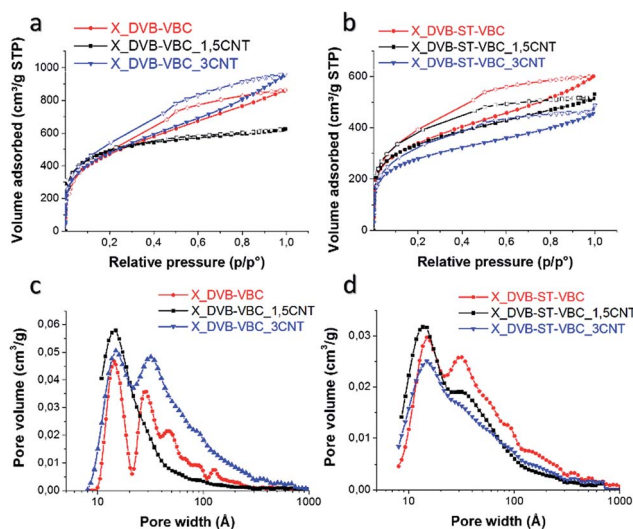

Fig. 6 Nitrogen adsorption (filled symbols) and desorption (empty symbols) isotherms at 77 K (a and b) and DFT pore size distribution (c and d) of the HCL resins and nanocomposites.

uptake values at 750 mmHg were obtained for the DVB–VBC and for the DVB–ST–VBC resins and nanocomposites. Moreover, the highest CO_2 adsorption values were obtained, for both the systems, at 1.5 phr MWCNT-PVBC loading, *i.e.* the samples showing the highest microporosity fractions.

Moreover, either the monomer composition, either the presence of modified nanotubes significantly affected the CO_2/N_2 selectivity. In particular, the X_DVB–ST–VBC resin showed higher selectivity in comparison to the X_DVB–VBC resin. This effect can be ascribed to the preferential interaction between CO_2 and the π-electron density of aromatic rings. Styrene resins have been already reported as selective systems toward CO_2 capture, even if their CO_2 adsorption capacity is quite low.[60]

Furthermore, as concerning HCL nanocomposites, for both systems a noteworthy improvement of the selectivity was obtained in presence of nanotubes, with selectivity values up to about 20 obtained for the X_DVB–ST–VBC_1.5CNT and X_DVB–ST–VBC_3CNT nanocomposite systems. Therefore, carbon nanotubes with their extended π-conjugation are able to further improve the CO_2 adsorption with respect to N_2.

All these results confirms a necessary trade-off between absolute adsorption and selectivity often registered in literature. In fact, simultaneous improvements in selectivity and absolute adsorption had been only generally obtained by introducing moieties able to enhance CO_2 binding affinities, like amines.[5,21,60,61] Nevertheless, there are many cases in which the increase of the selectivity occurs with a decrease of the overall CO_2 uptake. For instance, Dawson *et al.*[62] synthesized microporous copolymers starting from aniline and benzene. With increasing the content of aniline, CO_2/N_2 selectivity increases from 15.9 to 49.2 but CO_2 uptake decreases from 1.61 mmol g^{-1} to 0.35 mmol g^{-1}. In our systems, the best compromise was found for the nanocomposite system X_DVB–ST–VBC_1.5CNT, for which the recorded CO_2 uptake was found 0.80 mmol g^{-1} and the corresponding CO_2/N_2 selectivity was 20.9.

Nevertheless, for our systems there is still room for further functionalization of the MWCNT or the resin itself to promote even more selective CO_2/N_2 adsorption, but the obtained results indicate that the loading of nanotubes to low VBC content Davankov-type resins is a promising basis to realize highly selective systems.

H$_2$ adsorption. As widely stated, the spread of hydrogen for fuel applications is still limited by the lack of a cost-effective, efficient and safe method to store the gas. Research are currently underway to enhance H_2 absorption properties of organic materials.[63] The isosteric heat of H_2 adsorption for most carbonaceous materials is too low to enable significant adsorption phenomena at room temperature and H_2 adsorption is usually investigated at 77 K.[64] In this view, hydrogen adsorption analysis were performed at 77 K and up to 750 mmHg on the realized systems, in order to evaluate the effect of the monomer composition and the nanotube addition on the H_2 uptake of the resins. Results are reported in Table 1 and show adsorption values comparable to those reported in literature.[65–70] As already observed for the room temperature CO_2 uptake, H_2 uptake at 77 K is not directly correlated to the SSA, as

at 750 mmHg the X_DVB–VBC and the X_DVB–ST–VBC resins show comparable values of hydrogen adsorption. As concerning the effect of the nanotubes, MWCNT-PVBC inclusion was not able to induce significant changes in the hydrogen adsorption capacity of the X_DVB–ST–VBC resin, while it promoted an increased uptake for the X_DVB–VBC resin. By adding 1.5 or 3.0 phr of MWCNT-PVBC, the hyper-crosslinked DVB–VBC resin capacity increased by 25 or 21%, respectively. Both these HCL nanocomposites show higher SSA and room temperature CO_2 uptake with respect to the neat X_DVB–VBC resin, evidencing that the addition of nanotubes is able to improve the overall adsorption properties of the system.

Phenol extraction. Phenol extraction by using hyper-crosslinked resins is a promising approach for water purification.[58,71,72] The phenol adsorption capacity of these systems are affected by several factors including SSA, pore structure, and affinity between adsorbate and adsorbent.[73]

Phenol adsorption capacity of HCL resins and nanocomposites was evaluated by phenol extraction tests from water solutions. Fig. 7 shows the equilibrium phenol adsorption curves of the investigated materials. Adsorption equilibrium curves were fitted with the Freundlich equation

$$Q = K_F C^{1/n} \tag{1}$$

where Q (mmol kg^{-1}) is the amount of adsorbate extracted for unit mass of adsorbent, C (mmol L^{-1}) is the adsorbate concentration at equilibrium, K_F (mmol^{n-1} L^n kg^{-1}) is the Freundlich coefficient indicating the adsorption capacity and n is a parameter used as an indicator of the intensity of the adsorption. Higher the maximum capacity, higher the Freundlich coefficient. Lower the n value, more favorable is the adsorption.[17] The calculated Freundlich parameters K_F and n are reported in Table 2.

DVB–VBC resins and nanocomposites showed slightly higher adsorption capacity than the DVB–ST–VBC systems. In particular, X_DVB–VBC reaches values of adsorption comparable to those found in literature for similar resins.[17] By addition of 1.5 phr of MWCNT-PVBC an appreciable increase in phenol uptake was registered for both the compositions, with a corresponding increase of the K_F coefficient. At higher CNT loading, a decrease of the phenol adsorption capacity of the systems was recorded. It is noteworthy that X_DVB–ST–VBC_1.5CNT reaches values of adsorption higher than X_DVB–
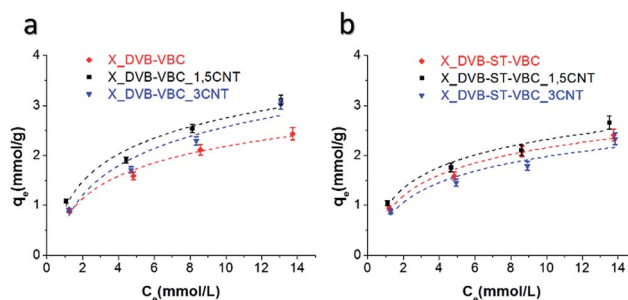

Fig. 7 Phenol adsorption isotherm measured at 298 K: (a) X_DVB–VBC systems; (b) X_DVB–ST–VBC systems.

Table 2 Freundlich parameters K_F and n calculated from the fitting of the phenol adsorption curves and corresponding correlation coefficients R^2

Sample	K_F	n	R^2
X_DVB–VBC	0.80	2.31	0.99
X_DVB–VBC_1.5CNT	1.04	2.36	0.97
X_DVB–VBC_3CNT	0.81	1.99	0.95
X_DVB–ST–VBC	0.87	2.56	0.98
X_DVB–ST–VBC_1.5CNT	1.00	2.75	0.96
X_DVB–ST–VBC_3CNT	0.78	2.51	0.94

VBC, even if X_DVB–ST–VBC_1.5CNT has significantly smaller specific surface area. As there is not a direct correlation between the SSA and the phenol uptake, the improved adsorption capacity of the systems containing 1.5 phr of nanotubes can be mainly ascribed to their higher microporosity, obtained as a consequence of the effective nanotube addition.

Conclusions

In this work properly modified multi-walled carbon nanotubes (MWCNT) were for the first time incorporated into a styrene/vinylbenzyl chloride/divinylbenzene hyper-crosslinked resin obtained by post-crosslinking of a lightly crosslinked type precursor. In order to promote the embedding of the nanotubes within the gel-type precursor, a proper surface modification strategy was set up, based on the grafting of a poly(vinylbenzyl chloride) (PVBC) resin onto the surface of the nanotubes, able to react with the resin, through the chloromethyl groups, during the hyper-crosslinking step.

FTIR spectroscopy evidenced that modified carbon nanotubes do not negatively affect neither the suspension polymerization of the lightly crosslinked resin, neither the hyper-crosslinking step. By addition of modified carbon nanotubes, a complex morphology of the precursor nanocomposite beads was revealed by SEM analysis.

Carbon nanotubes slightly affect the SSA of the final resins, with moderate changes recorded as a function of the nanofiller loading and the composition of the resin. Nevertheless, for both the investigated compositions, at low nanofiller loadings a significant increase of the microporosity fraction was observed, up to 64% for the sample X_DVB–VBC_1.5CNT, that also showed improved CO_2 uptake (up to 3.55 wt%) and H_2 uptake (up to 1.39 wt%). Interestingly, also for the system X_DVB–ST–VBC, containing the styrene co-monomer and showing lower SSA, at 1.5 wt% CNT loading, an increase of the CO_2 uptake was recorded, reaching values comparable to those obtained for the X_DVB–VBC systems.

Moreover, despite the absence of proper functionalization strategies aimed at inserting moieties with high affinity towards CO_2, the addition of nanotubes also promoted an increase of the CO_2/N_2 selectivity, thus indicating that the embedding in Davankov-type resins of carbon nanotubes, characterized by their extended π-conjugation, is a promising approach to realize highly selective systems towards CO_2 absorption.

Finally, preliminary tests of phenol adsorption from water solutions were carried out to evaluate possible applications of the investigated systems for water remediation. Also in this case, the addition of carbon nanotubes to the resins was able to improve the overall adsorption capacity of phenol, in particular for the DVB–VBC system.

All these results confirm that the addition of the properly surface modified carbon based nanofillers, able to interact with the hosting resin during the synthesis of the precursor and to participate to the hyper-crosslinking reaction, is a promising approach to modulate and improve either the gas sorption properties either the removal ability of organic contaminants from water of styrene/vinylbenzyl chloride/divinylbenzene microporous polymers.

References

1 A. Dąbrowski, P. Podkościelny, Z. Hubicki and M. Barczak, *Chemosphere*, 2005, **58**, 1049.
2 J. Weitkamp, *Solid State Ionics*, 2000, **131**, 175.
3 J. L. C. Rowsell and O. M. Yaghi, *Microporous Mesoporous Mater.*, 2004, **73**, 3.
4 H. Furukawa, N. Ko, Y. B. Go, N. Aratani, S. B. Choi, E. Choi, A. Ö. Yazaydin, R. Q. Snurr, M. O'Keeffe, J. Kim and O. M. Yaghi, *Science*, 2010, **329**, 424.
5 H. A. Patel, S. H. Je, J. Park, D. P. Chen, Y. Jung, C. T. Yavuz and A. Coskun, *Nat. Commun.*, 2013, **4**, 1357.
6 S.-Y. Ding, J. Gao, O. Wang, Y. Zhang, W.-G. Song, C.-Y. Su and W. Wang, *J. Am. Chem. Soc.*, 2011, **133**, 19816.
7 N. B. McKeown and P. M. Budd, *Chem. Soc. Rev.*, 2006, **35**, 675.
8 J. Lee, C. D. Wood, D. Bradshaw, M. J. Rosseinsky and A. I. Cooper, *Chem. Commun.*, 2006, **25**, 2670.
9 D. Lin and B. Xing, *Environ. Sci.*, 2008, **42**, 7254.
10 P. Bernardo, E. Drioli and G. Golemme, *Ind. Eng. Chem. Res.*, 2009, **48**, 4638.
11 H. Yang, Z. Xu, M. Fan, R. Gupta, R. B. Slimane, A. E. Bland and I. Wright, *J. Environ. Sci.*, 2008, **20**, 14.
12 R. T. Yang, *Gas Separation by Adsorption Processes*, Butterworth Publishers, Stoneham, 2013.
13 R. Dawson, A. I. Cooper and D. J. Adams, *Prog. Polym. Sci.*, 2012, **37**, 530.
14 R. E. Morris and P. S. Wheatley, *Angew. Chem., Int. Ed.*, 2008, **47**, 4966.
15 A. Corma, *Chem. Rev.*, 1997, **97**, 2373.
16 C. F. Martín, E. Stöckel, R. Clowes, D. J. Adams, A. I. Cooper, J. J. Pis, F. Rubiera and C. Pevida, *J. Mater. Chem.*, 2011, **21**, 5475.
17 A. Li, Q. Zhang, G. Zhang, J. Chen, Z. Fei and F. L. Li, *Chemosphere*, 2002, **47**, 981.
18 K. Yang, W. Wu, Q. Jing and L. Zhu, *Environ. Sci. Technol.*, 2008, **42**, 7931.
19 X. Wang, P. D. Patil, C. He, J. Huang and Y.-N. Liu, *J. Appl. Polym. Sci.*, 2015, **132**, 41597.
20 R. T. Woodward, L. A. Stevens, R. Dawson, M. Vijayaraghavan, T. Hasell, I. P. Silverwood, A. V. Ewing, T. Ratvijitvech, J. D. Exley, S. Y. Chong, F. Blanc,

D. J. Adams, S. G. Kazarian, C. E. Snape, T. C. Drage and A. I. Cooper, *J. Am. Chem. Soc.*, 2014, **136**, 9028.

21 R. Dawson, A. I. Cooper and D. J. Adams, *Polym. Int.*, 2013, **62**, 345.

22 R. Dawson, L. A. Stevens, T. C. Drage, C. E. Snape, M. W. Smith, D. J. Adams and A. I. Cooper, *J. Am. Chem. Soc.*, 2012, **134**, 10741.

23 J. Germain, F. Svec and J. M. J. Fréchet, *Chem. Mater.*, 2008, **20**, 7069.

24 R. Dawson, E. Stöckel, J. R. Holst, D. J. Adams and A. I. Cooper, *Energy Environ. Sci.*, 2011, **4**, 4239.

25 N. Fontanals, J. Cortés, M. Galià, R. M. Marcé, P. A. G. Cormack, F. Borrull and D. C. Sherrington, *J. Polym. Sci., Part A: Polym. Chem.*, 2005, **43**, 1718.

26 N. Fontanals, R. M. Marcé, F. Borrull and P. A. G. Cormack, *Polym. Chem.*, 2015, **6**, 7231.

27 S. Shen, X. Zhang and L. Fan, *Mater. Lett.*, 2008, **62**, 2392.

28 M. P. Tsyurupa and V. A. Davankov, *React. Funct. Polym.*, 2006, **66**, 768.

29 Q.-Q. Liu, L. Wang, A.-G. Xiao, H.-J. Yu and Q.-H. Tan, *Eur. Polym. J.*, 2008, **44**, 2516.

30 J.-H. Ahn, J.-E. Jang, C.-G. Oh, S.-K. Ihm, J. Cortez and D. C. Sherrington, *Macromolecules*, 2006, **39**, 627.

31 L. Jia, X. Song, J. Wu and C. Long, *J. Phys. Chem. C*, 2015, **119**, 21404.

32 X. Li, Y. Liu, D. Di, G. Wang and Y. Liu, *Colloids Surf., A*, 2016, **500**, 1.

33 X. Zeng, H. Chen, Y. Zheng, W. Tao, Y. Fan, L. Huang and L. Mei, *J. Colloid Interface Sci.*, 2012, **385**, 166.

34 X. Zeng, T. Yu, P. Wang, R. Yuan, Q. Wen, Y. Fan, C. Wang and R. Shi, *J. Hazard. Mater.*, 2010, **177**, 773.

35 X. Zeng, Y. Fan, G. Wu, C. Wang and R. Shi, *J. Hazard. Mater.*, 2009, **169**, 1022.

36 X. Ling, H. Li, H. Zha, C. He and J. Huang, *Chem. Eng. J.*, 2016, **286**, 400.

37 Q. B. Meng and J. Weber, *ChemSusChem*, 2014, **7**, 3312.

38 W. Wang, Y. Ma, Q. Zhou, C. Shuang, M. Zhang and A. Li, *Front. Environ. Sci. Eng.*, 2015, **9**, 96.

39 M. J. Allen, V. C. Tung and R. B. Kaner, *Chem. Rev.*, 2010, **110**, 132.

40 F. L. Darkrim, P. Malbrunot and G. P. Tartaglia, *Int. J. Hydrogen Energy*, 2002, **27**, 193.

41 X. Ren, C. Chen, M. Nagatsu and X. Wang, *Chem. Eng. J.*, 2011, **170**, 395.

42 J. Zhao, A. Buldum, J. Han and J. P. Lu, *Nanotechnology*, 2002, **13**, 195.

43 C.-H. Yu, C.-H. Huang and C.-S. Tan, *Aerosol Air Qual. Res.*, 2012, **12**, 745.

44 S. Agnihotri, M. J. Rood and M. Rostam-Abadi, *Carbon*, 2005, **43**, 2379.

45 R. Q. Long and R. T. Yang, *J. Am. Chem. Soc.*, 2001, **123**, 2058.

46 Y. H. Li, S. Wang, Z. Luan, J. Ding, C. Xu and D. Wu, *Carbon*, 2003, **41**, 1057.

47 F. Su and C. Lu, *J. Environ. Sci. Health, Part A: Toxic/Hazard. Subst. Environ. Eng.*, 2007, **42**, 1543.

48 F. Su, C. Lu, W. Cnen, H. Bai and J. F. Hwang, *Sci. Total Environ.*, 2009, **407**, 3017.

49 X. Chen, M. Zhou, Q. Hou, X. Tu and X. Wu, *Macromol. Chem. Phys.*, 2013, **214**, 1829.

50 J. Landers, G. Y. Gor and A. V. Neimark, *Colloids Surf., A*, 2013, **437**, 3.

51 P. B. Nagabalasubramanian, S. Periandy and S. Mohan, *Spectrochim. Acta, Part A*, 2010, **77**, 150.

52 V. Ambrogi, G. Gentile, C. Ducati, M. C. Oliva and C. Carfagna, *Polymer*, 2012, **53**, 291.

53 G. Nasti, G. Gentile, P. Cerruti, C. Carfagna and V. Ambrogi, *Polymer*, 2016, **99**, 193.

54 N. M. Briggs, J. S. Weston, B. Li, D. Venkataramani, C. P. Aichele, J. H. Harwell and S. P. Crossley, *Langmuir*, 2015, **31**, 13077.

55 M. P. Tsyurupa and V. A. Davankov, *React. Funct. Polym.*, 2002, **53**, 193.

56 G. Meng, A. Li, W. Yang, F. Liu, X. Yang and Q. Zhang, *Eur. Polym. J.*, 2007, **43**, 2732.

57 M. P. Tsyurupa, Z. K. Blinnikova, Y. A. Davidovich, S. E. Lyubimov, A. V. Naumkin and V. A. Davankov, *React. Funct. Polym.*, 2012, **72**, 973.

58 V. V. Azanova and J. Hradil, *React. Funct. Polym.*, 1999, **41**, 163.

59 P. I. Ravikovitch, S. C. Ó. Domhnaill, A. V. Neimark, F. Schüth and K. K. Unger, *Langmuir*, 1995, **11**, 4765.

60 R. Evans, U. M. B. Marconi and P. Tarazona, *J. Chem. Soc., Faraday Trans. 2*, 1986, **82**, 1763.

61 J. Wang, J. G. W. Yang, G. Yi and Y. Zhang, *Chem. Commun.*, 2015, **51**, 15708.

62 R. Dawson, T. Ratvijitvech, M. Corker, A. Laybourn, Y. Z. Khimyak, A. I. Cooper and D. J. Adams, *Polym. Chem.*, 2012, **3**, 2034.

63 L. Pan, Q. Chen, J.-H. Zhu, J.-C. Yu, Y.-J. He and B.-H. Han, *Polym. Chem.*, 2015, **6**, 2478.

64 C. D. Wood, B. Tan, A. Trewin, H. Niu, D. Bradshaw, M. J. Rosseinsky, Y. Z. Khimyak, N. L. Campbell, R. Kirk, E. Stöckel and A. I. Cooper, *Chem. Mater.*, 2007, **19**, 2034.

65 J. Germain, J. Hradil, J. M. J. Fréchet and F. Svec, *Chem. Mater.*, 2006, **18**, 4430.

66 B. Li, R. Gong, W. Wang, X. Huang, W. Zhang, H. Li, C. Hu and B. Tan, *Macromolecules*, 2011, **44**, 2410.

67 K. M. Thomas, *Catal. Today*, 2007, **120**, 389.

68 H. Furukawa and O. M. Yaghi, *J. Am. Chem. Soc.*, 2009, **131**, 8875.

69 B. Panella, M. Hirscher and S. Roth, *Carbon*, 2005, **43**, 2209.

70 E. Poirier, R. Chahine and T. K. Bose, *Int. J. Hydrogen Energy*, 2001, **26**, 831.

71 J. Huang, X. Jin and S. Deng, *Chem. Eng. J.*, 2012, **192**, 192.

72 X. Zhang, A. Li, Z. Jiang and Q. Zhang, *J. Hazard. Mater.*, 2006, **137**, 1115.

73 K. Yang and B. Xing, *Chem. Rev.*, 2010, **110**, 5989.

This journal is © The Royal Society of Chemistry 2017